https://doi.org/10.1016/j.jnoncrysol.2017.03.016

Large adiabatic temperature rise above the water ice point of a minor Fe substituted $Gd_{50}Co_{50}$ amorphous alloy

B. Z. Tang[1, 2], D. Q. Guo[2], D. Ding[1, 2], L. Xia[1, *] and K. C. Chan[2, *]

[1] Laboratory for Microstructure, Institute of Materials, Shanghai University, Shanghai 200072, China &

[2] Department of Industrial and Systems Engineering, The Hong Kong Polytechnic University, Hung Hom, Hong Kong

Abstract

In this study, we have successfully improved the Curie temperature of $Gd_{50}Co_{50}$ amorphous alloy from 267 K to 277 K by a minor Fe addition as a replacement for Co. The $Gd_{50}Co_{48}Fe_2$ as-spun ribbons exhibit typical characteristics of a soft magnetic amorphous alloy. The magnetic entropy change peak for this amorphous alloy was slightly decreased by the minor Fe addition, but the adiabatic temperature rise (ΔT_{ad}) of the $Gd_{50}Co_{48}Fe_2$ amorphous alloy is comparable to that of the $Gd_{50}Co_{50}$ amorphous alloy, both of which are larger than those of other metallic glasses near the ice point of water. The maximum ΔT_{ad} of the $Gd_{50}Co_{48}Fe_2$ amorphous ribbon at 277.5 K is about 1.44 K under 1 T, 2.44 K under 2 T, 3.31 K under 3 T, 4.1 K under 4 T and about 4.84 K under 5 T. The large maximum value of ΔT_{ad} above the ice point indicates that the $Gd_{50}Co_{48}Fe_2$ amorphous alloy could be an ideal candidate for the high efficient magnetic refrigerant in a household refrigerator.

Keywords: metallic amorphous alloy, element substitution, magneto-caloric effect, adiabatic temperature rise

[*] Corresponding authors. Email: xialei@shu.edu.cn (L. Xia) and kc.chan@polyu.edu.hk (K. C. Chan)

1. Introduction

Magnetic refrigeration (MR) based on the magneto-caloric effect (MCE) of magnetic materials has attracted increasing interests because it is more compact, more effective, safes for the environment and has lower energy consumption than the traditional vapor-cycle refrigeration [1-5]. In the last two decades, MR working materials have been studied intensively and numerous MCE alloys have been developed [5-24]. Among these MCE materials, some intermetallic compounds such as $Gd_5(Si_2Ge_2)$, $MnFeP_{0.45}As_{0.55}$, $MnAs_{1-x}Sb_x$ and $Ni_{52.6}Mn_{23.1}Ga_{24.3}$, show a sharp magnetic entropy change ($-\Delta S_m$) peak due to their first order magnetic phase transition [5-9]; in contrast, metallic glasses and some crystalline alloys (e.g., Gd, $Gd_6Co_2Si_3$ and so on) exhibit a broadened $-\Delta S_m$ peak because they undergo a second order magnetic phase transition [10-24]. Except for the relatively lower peak values of $-\Delta S_m$ ($-\Delta S_m^{peak}$), almost all the features of metallic glasses are superior to crystalline alloys: ultrahigh refrigeration capacity (RC), which is several times higher than that in crystalline alloys; tunable Curie temperature (T_c) without dramatic deterioration of MCE within a large compositional range; low hysteresis loss and low current eddy loss; excellent mechanical properties and good corrosion resistance [12-24]. It is therefore important to improve the $-\Delta S_m^{peak}$ values of amorphous MCE alloys, especially near room temperature.

Although some of the Gd-based metallic glasses exhibit higher $-\Delta S_m^{peak}$ and even much higher RC than those of the pure Gd, their T_c values are far from room temperature [15-20]. The $-\Delta S_m^{peak}$ values of Fe-based amorphous alloys, however, are not high enough for use as magnetic refrigerants even though they exhibit a T_c around room temperature [12-14]. Currently, we have prepared $Gd_{50}Co_{50}$ binary amorphous ribbons with excellent magneto-caloric properties near the freezing temperature of water [21]. This binary metallic glass exhibits a large $-\Delta S_m^{peak}$ and adiabatic temperature rise (ΔT_{ad}) peak at about 267 K. On the other hand, the $Gd_{48}Co_{52}$ binary amorphous ribbons exhibit a ΔT_{ad} peak comparable to that of $Gd_{50}Co_{50}$ metallic glass above the ice point of water, but is hard to be fabricated due to its poor glass forming ability (GFA) [22]. Although the T_c of binary $Gd_{50}Co_{50}$ amorphous alloy has been successfully improved to nearly 290 K by adding 5% (at. %) Fe as a replacement of Co in the binary glass forming alloy, the $-\Delta S_m^{peak}$ of the $Gd_{50}Co_{45}Fe_5$ decreased dramatically [23]. Considering the application of metallic glasses as magnetic refrigerants for a household refrigerator, it is more important to develop amorphous MCE alloys with a high $-\Delta S_m^{peak}$ value above the freezing temperature of water. In the present work, we add small amount of Fe as a replacement for Co in the $Gd_{50}Co_{50}$ binary amorphous alloy in an attempt to improve the T_c to the temperature to above the ice point of water, and at the same time keep the ΔT_{ad} of the $Gd_{50}Co_{48}Fe_2$ metallic glass comparable to the that of the $Gd_{50}Co_{50}$ binary amorphous alloy. The magnetic properties as well as the magneto-caloric behavior of the $Gd_{50}Co_{48}Fe_2$ amorphous alloy were studied in detail.

2. Experimental procedure

A $Gd_{50}Co_{48}Fe_2$ ingot was prepared by arc-melting a mixture of Gd, Co and Fe metals with purities above 99.9% (at. %) and re-melting for least four times in a water cooled copper crucible under a Ti-gettered argon atmosphere. $Gd_{50}Co_{48}Fe_2$ as-spun ribbons were prepared by melt-spinning on a single copper wheel with a linear speed of about 30 m/s under a pure argon atmosphere. The amorphous structure of the $Gd_{50}Co_{48}Fe_2$ as-spun ribbon was ascertained by a Rigaku D\max-2550 X-ray diffractometer (XRD) using Cu K_α radiation. The differential scanning calorimetry (DSC) curve of the $Gd_{50}Co_{48}Fe_2$ amorphous ribbon was measured at a heating rate of 20 K/min using a Perkin-Elmer DIAMOND DSC under a purified argon atmosphere. The heat capacity and magnetic properties of the $Gd_{50}Co_{48}Fe_2$ amorphous ribbon were measured by a Physical Properties Measurement System (Quantum Design PPMS 6000).

3. Results and discussion

Figure 1 shows the XRD pattern of the $Gd_{50}Co_{48}Fe_2$ and $Gd_{50}Co_{50}$ as-spun ribbons. The $Gd_{50}Co_{50}$ as-spun ribbon was also prepared at a surface speed of 30 m/s.

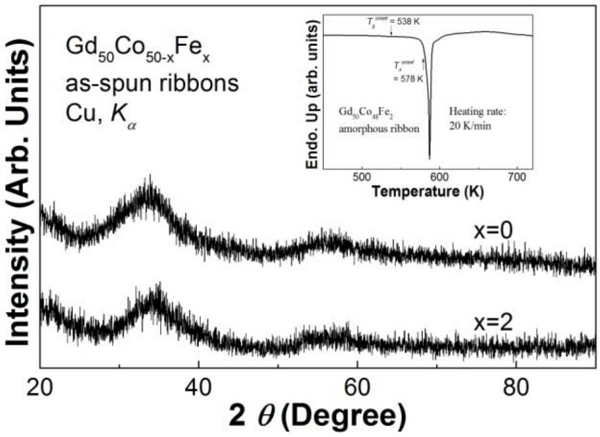

Figure 1. XRD patterns of the $Gd_{50}Co_{48}Fe_2$ and $Gd_{50}Co_{50}$ as-spun ribbons

The ribbons show the typical amorphous structures of a broadened hump without any sharp peaks of crystalline phases on the XRD patterns. The glass transition and crystallization behavior, as typical characteristics of amorphous alloys, are also found in the DSC trace of the as-spun $Gd_{50}Co_{48}Fe_2$ ribbon, as shown in the inset of Fig. 1. The $Gd_{50}Co_{48}Fe_2$ alloy can easily be fabricated in ribbon or wire shape, which can achieve a larger heat exchange efficiency and a lower eddy current loss than their bulk counterparts [21-22, 25].

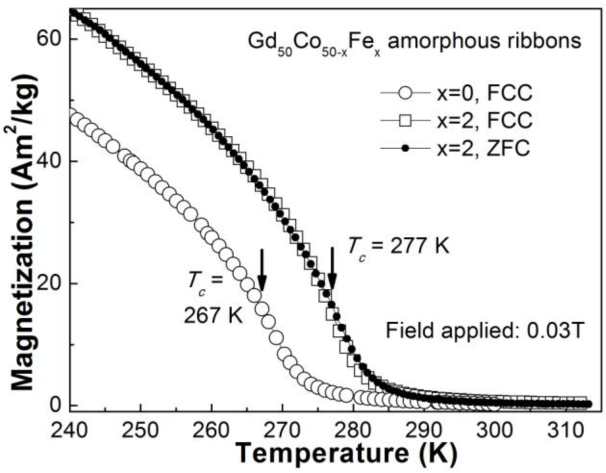

Figure 2 The FCC and ZFC M-T curves for the $Gd_{50}Co_{48}Fe_2$ amorphous ribbon, and the FCC and ZFC M-T curve for the $Gd_{50}Co_{50}$ amorphous ribbon under a field of 0.03 T.

Figure 2 shows the temperature dependence of zero field cooled (ZFC) and field cooled (FCC) magnetization (M-T) curves of the $Gd_{50}Co_{48}Fe_2$ amorphous ribbon under a field of 0.03 T, and the FCC M-T curve of the $Gd_{50}Co_{50}$ amorphous ribbon under the same magnetic field for comparison purposes. For the $Gd_{50}Co_{48}Fe_2$ amorphous alloy, the ZFC M-T curve is almost the same as the FCC M-T curve. The T_c of the $Gd_{50}Co_{48}Fe_2$ amorphous ribbon, marked clearly on the *M-T* curve, is about 277 K. Clearly, the T_c of the $Gd_{50}Co_{50}$ amorphous alloy can be enhanced by a small Fe addition, and in particular, the T_c of the $Gd_{50}Co_{48}Fe_2$ metallic glass is about 4 K higher than the ice point of water.

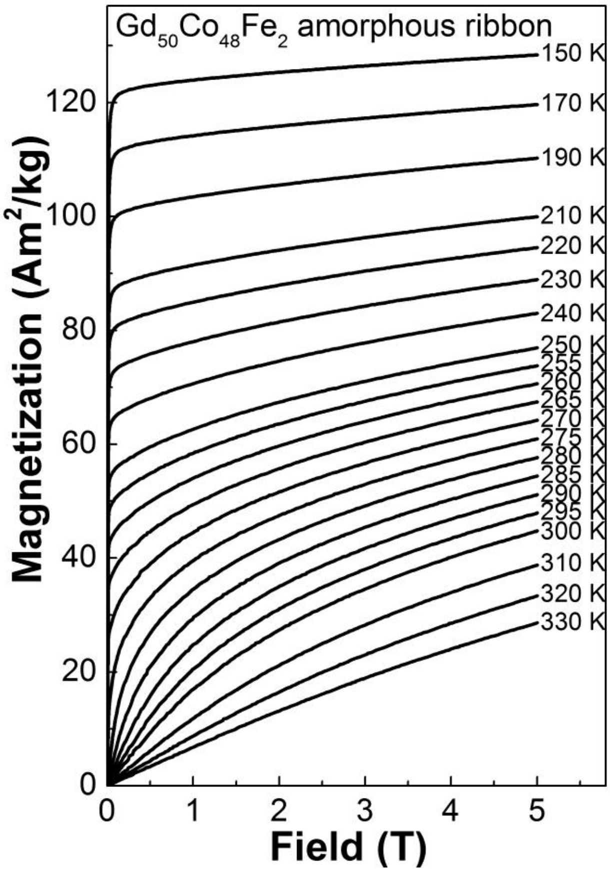

Figure 3. The isothermal magnetization (*M-H*) curves of the $Gd_{50}Co_{48}Fe_2$ amorphous ribbon at different temperatures ranging from 150 K to 330 K.

Figure 3 shows the isothermal magnetization (*M-H*) curves of the $Gd_{50}Co_{48}Fe_2$ amorphous ribbon at different temperatures ranging from 150 K to 330 K. Therefore, the temperature dependence of $-\Delta S_m$ ($(-\Delta S_m)$-T) curves of the $Gd_{50}Co_{48}Fe_2$ amorphous ribbon under various magnetic fields can be derived from their *M-H* curves, and are shown in Fig. 4. The -ΔS_m^{peak} value of the $Gd_{50}Co_{48}Fe_2$ amorphous ribbon is about 1.32 $Jkg^{-1}K^{-1}$ under 1 T, 2.24 $Jkg^{-1}K^{-1}$ under 2 T, 3.04 $Jkg^{-1}K^{-1}$ under 3 T, 3.76 $Jkg^{-1}K^{-1}$ under 4 T and 4.44 $Jkg^{-1}K^{-1}$ under 5 T at 277.5 K. Compared to the Gd-Co-based amorphous alloys with a Gd concentration around 50% (at. %), the -ΔS_m^{peak} of the

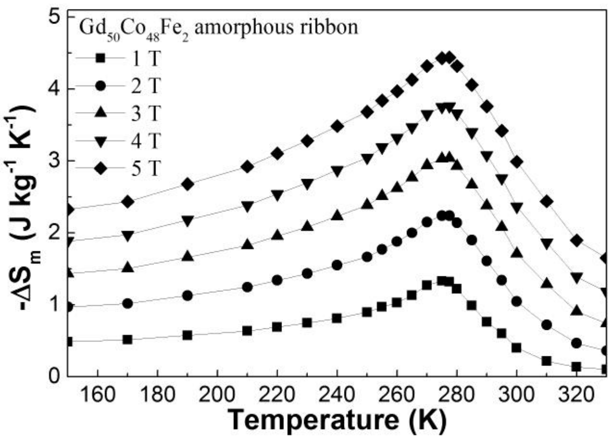

Figure 4. The temperature dependence of -ΔS_m ((-ΔS_m)-*T*) curves of the $Gd_{50}Co_{48}Fe_2$ amorphous ribbon under various magnetic fields.

$Gd_{50}Co_{48}Fe_2$ amorphous ribbon is lower than those of the $Gd_{50}Co_{48}Zn_2$ amorphous ribbon (5.04 $Jkg^{-1}K^{-1}$ under 5 T at 260 K), the $Gd_{48}Co_{50}Zn_2$ amorphous ribbon (5.02 $Jkg^{-1}K^{-1}$ under 5 T at 262 K) [24], the $Gd_{50}Co_{48}Mn_2$ amorphous ribbon (5.24 $Jkg^{-1}K^{-1}$ under 5 T at 258 K, unpublished data), the $Gd_{50}Co_{45}Mn_5$ amorphous ribbon (5.49 $Jkg^{-1}K^{-1}$ under 5 T at 245 K, unpublished data) and the $Gd_{50}Co_{50}$ amorphous ribbon (4.6 $Jkg^{-1}K^{-1}$ under 5 T at 267 K) [21], but is higher than the -ΔS_m^{peak} of the $Gd_{48}Co_{52}$ amorphous ribbon (4.23 $Jkg^{-1}K^{-1}$ under 5 T at 280 K) and the $Gd_{50}Co_{45}Fe_5$ amorphous ribbon (3.8 $Jkg^{-1}K^{-1}$ under 5 T at 289.5 K) [22-23]. It can be noticed that the peak values of -ΔS_m of these Gd-Co-based amorphous alloys decrease obviously with the increase of their T_c. According to the relationship between -ΔS_m^{peak} and T_c proposed from the mean field theory [26], we constructed the -ΔS_m^{peak}-$T_c^{-2/3}$ plots for the $Gd_{50}Co_{50}$, $Gd_{48}Co_{52}$, $Gd_{50}Co_{48}Zn_2$, $Gd_{48}Co_{50}Zn_2$, $Gd_{50}Co_{48}Mn_2$, $Gd_{50}Co_{45}Mn_5$, $Gd_{50}Co_{48}Fe_2$ and $Gd_{50}Co_{45}Fe_5$ amorphous ribbons, as shown in Fig. 5. The nearly linear fitting of the $-\Delta S_m^{peak}$-$T_c^{-2/3}$ plots (the dash line in Fig. 5) indicates that the $-\Delta S_m^{peak}$ of the $Gd_{50}Co_{48}Fe_2$ amorphous ribbon is mainly determined by its Curie temperature.

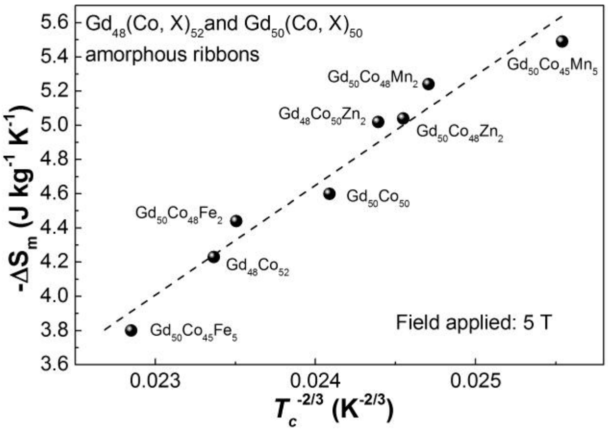

Figure 5. the $-\Delta S_m^{peak}$-$T_c^{-2/3}$ plots for the $Gd_{50}Co_{50}$, $Gd_{48}Co_{52}$, $Gd_{50}Co_{48}Zn_2$, $Gd_{48}Co_{50}Zn_2$, $Gd_{50}Co_{48}Mn_2$, $Gd_{50}Co_{45}Mn_5$, $Gd_{50}Co_{48}Fe_2$ and $Gd_{50}Co_{45}Fe_5$ amorphous ribbons

The magneto-caloric behavior of the $Gd_{50}Co_{48}Fe_2$ as-spun ribbon is illustrated by the field dependence of $-\Delta S_m$, which follows a $-\Delta S_m \propto H^n$ relationship. Figure 6 shows the linear fitting of $\ln(-\Delta S_m^{peak})$ *vs* $\ln(H)$ and the inset shows the temperature dependence of n (n-T) curve for the $Gd_{50}Co_{48}Fe_2$ as-spun ribbon. The $Gd_{50}Co_{48}Fe_2$

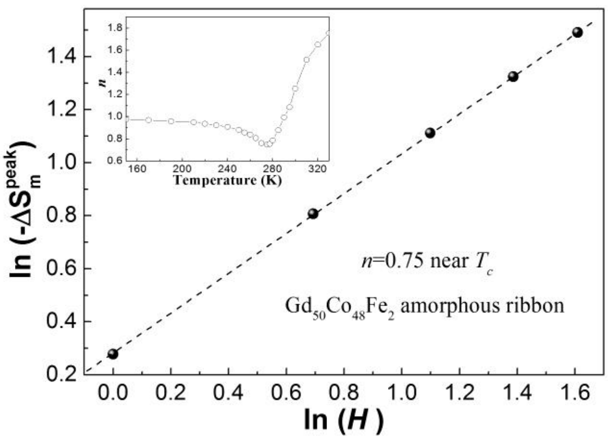

Figure 6. The linear fitting of $\ln(-\Delta S_m^{peak})$ *vs* $\ln(H)$ and the inset shows the temperature dependence of n (n-T) curve for the $Gd_{50}Co_{48}Fe_2$ as-spun ribbon.

as-spun ribbon exhibits the typical characteristics of soft magnetic amorphous materials: $n \approx 1$ at a temperature well below T_c; n is close to 2 in the paramagnetic range; and n=0.75 near T_c. The n value near T_c of the $Gd_{50}Co_{48}Fe_2$ as-spun ribbon is larger than the theoretical one proposed by H. Oesterreicher and F. T. Parker [27], but is very close to the one derived from the Arrott-Noakes equation by V. Franco *et al.* [28], indicating that the magneto-caloric behavior of the $Gd_{50}Co_{48}Fe_2$ as-spun ribbon is similar to other fully amorphous alloys with only short-range order embedded in the disordered matrix.

It is difficult to compare the refrigeration efficiency between the $Gd_{50}Co_{48}Fe_2$ and $Gd_{50}Co_{50}$ amorphous ribbons because of their different working temperature due to their different T_c values. Therefore, we employed a more direct gauge, ΔT_{ad}, to evaluate the cooling efficiency of these amorphous alloys under the same magnetic field. The dependence of ΔT_{ad} on the temperature of the amorphous alloys (ΔT_{ad}-T curve) under a magnetic field can be calculated as follows:

$$\Delta T_{ad}(T,0 \to H) = -\frac{T}{C_p(T)} \Delta S_m(T,0 \to H)$$

The C_p-T curve for $Gd_{50}Co_{48}Fe_2$ amorphous ribbon is shown in the inset of Fig. 7. Thus, combining the (-ΔS_m)-T and C_p-T curves, we determine the ΔT_{ad}-T curve of $Gd_{50}Co_{48}Fe_2$, as shown in Fig. 7. The maximum ΔT_{ad} of the $Gd_{50}Co_{48}Fe_2$ amorphous ribbon at 277.5 K is about 1.44 K under 1 T, 2.44 K under 2 T, 3.31 K under 3 T, 4.1 K under 4 T and about 4.84 K under 5 T.

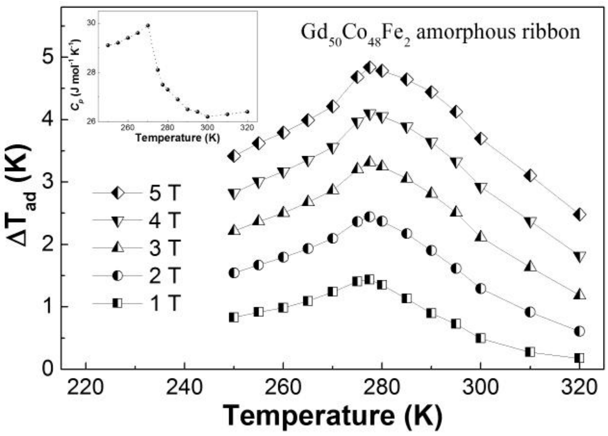

Figure 7. The ΔT_{ad}-T curve of $Gd_{50}Co_{48}Fe_2$ amorphous ribbon and the inset shows its C_p-T curve

Although the -ΔS_m^{peak} of $Gd_{50}Co_{48}Fe_2$ amorphous ribbon is slightly lower than that of the $Gd_{50}Co_{50}$ amorphous ribbon, the maximum ΔT_{ad} of the $Gd_{50}Co_{48}Fe_2$ amorphous ribbon is still comparable to that of the $Gd_{50}Co_{50}$ amorphous ribbon, and is larger than those of other metallic glasses with T_c near room temperature [21]. Considering that the T_c value of the $Gd_{50}Co_{48}Fe_2$ amorphous ribbon is higher than the freezing temperature of water, the $Gd_{50}Co_{48}Fe_2$ amorphous ribbon is more suitable for application as a magnetic refrigerant in an energy efficient household refrigerator.

4. Conclusions

In summary, we obtained $Gd_{50}Co_{48}Fe_2$ amorphous alloys with improved T_c above the ice point. The -ΔS_m^{peak} of the $Gd_{50}Co_{48}Fe_2$ amorphous ribbon, which is closely related to its T_c value according to mean field theory, is found to be slightly lower than that of the $Gd_{50}Co_{50}$ amorphous ribbon. The *n* -T curve of the $Gd_{50}Co_{48}Fe_2$ glassy ribbon illustrates the typical magneto-caloric behavior of soft magnetic metallic glasses. The maximum ΔT_{ad} of $Gd_{50}Co_{48}Fe_2$ metallic glass is larger than those of other amorphous alloys with T_c above the freezing temperature of water, indicating that the amorphous ribbon is an ideal candidate for use as a highly efficient magnetic refrigerant in a household refrigerator.

Acknowledgments

The work described in this paper was supported by the Research Grants Council of the Hong Kong Special Administrative Region, China (Project No. PolyU 511212).

References

1. A. M. Tishin and Y. I. Spichkin (2003) The Magnetocaloric Effect and Its Applications, Institute of Physics Publishing Ltd., Bristol
2. N. A. de Oliveira, P. J. von Ranke (2009) Theoretical aspects of the magnetocaloric effect. Phys. Rep. 489:89-159. doi: 10.1016/j.physrep.2009.12.006
3. E. Brück (2005) Developments in magnetocaloric refrigeration. J. Phys. D: Appl. Phys. 38:R381-391. doi: 10.1088/0022-3727/38/23/R01
4. J. Glanz (1998) Making a Bigger Chill With Magnets. Science. 279:2045. doi: 10.1126/science.279.5359.2045
5. K. A. Gschneider, V. K. Pecharsky, Jr., A. O. Tsokol (2005) Recent developments in magnetocaloric materials. Rep. Prog. Phys. 68:1479-1539. doi: 10.1088/0034-4885/68/6/r04
6. L. Morellon, J. Blasco, P. A. Algarabel and M. R. Ibarra (2000) Nature of the first-order antiferromagnetic-ferromagnetic transition in the Ge-rich magnetocaloric compounds $Gd_5(Si_xGe_{1-x})_4$. Phys. Rev. B 62:1022-1026. doi: 10.1103/PhysRevB.62.1022
7. H. Wada and Y. Tanabe (2001) Giant magnetocaloric effect of $MnAs_{1-x}Sb_x$. Appl. Phys. Lett. 79:3302-3304. doi: 10.1063/1.1419048
8. F. Hu, B. Shen, J. Sun, G. Wang and Z. Cheng (2002) Very large magnetic entropy change near room temperature in $LaFe_{11.2}Co_{0.7}Si_{1.1}$. Appl. Phys. Lett. 80:826-828. doi: 10.1063/1.1447592
9. S. Stadler, M. Khan, J. Mitchell, N. Ali, A. M. Gomes, I. Dubenko, A. Y. Takeuchi and A. P. Guimarães (2006) Magnetocaloric properties of $Ni_2Mn_{1-x}Cu_xGa$. Appl. Phys. Lett. 88:192511. doi: 10.1063/1.2202751
10. G. V. Brown (1976) Magnetic heat pumping near room temperature. J. Appl. Phys. 47:3673-3680. doi: 10.1063/1.323176
11. J. Sun, J. F. Wu and J. R. Sun (2009) Room-temperature large refrigerant capacity of $Gd_6Co_2Si_3$. J. Appl. Phys. 106:083902. doi: 10.1063/1.3243289

12. V. Franco, C. F. Conde, A. Conde and L. F. Kiss (2007) Enhanced magnetocaloric response in Cr/Mo containing Nanoperm-type amorphous alloys. Appl. Phys. Lett. 90:052509. doi: 10.1063/1.2437659
13. P. Alvarez-Alonso, J. L. Sanchez Llamazares, C. F. Sanchez-Valdes, M. L. FdezGubieda, P. Gorria and J. A. Blanco (2015) High-magnetic field characterization of magnetocaloric effect in FeZrB(Cu) amorphous ribbons. J. Appl. Phys. 117:17A710. doi: 10.1063/1.4907188
14. S. Atalay, H. Gencer and V. S. Kolat (2005) Magnetic entropy change in $Fe_{74-x}Cr_xCu_1Nb_3Si_{13}B_9$ (x = 14 and 17) amorphous alloys. J. Non-Cryst. Solids. 351:2373-2377. doi:10.1016/j.jnoncrysol.2005.07.012
15. Q. Luo, D. Q. Zhao, M. X. Pan and W. H. Wang (2006) Magnetocaloric effect in Gd-based bulk metallic glasses. Appl. Phys. Lett. 89:081914. doi: 10.1063/1.2338770
16. J. Du, Q. Zheng, Y. B. Li, Q. Zhang, D. Li, Z. D. Zhang (2008) Large magnetocaloric effect and enhanced magnetic refrigeration in ternary Gd-based bulk metallic glasses. J. Appl. Phys. 103:023918. doi: 10.1063/1.2836956
17. F. Yuan, J. Du and B. Shen (2012) Controllable spin-glass behavior and large magnetocaloric effect in Gd-Ni-Al bulk metallic glasses. Appl. Phys. Lett. 101: 032405. doi: 10.1063/1.4738778
18. L. Xia, M. B. Tang, K. C. Chan and Y. D. Dong (2014) Large magnetic entropy change and adiabatic temperature rise of a $Gd_{55}Al_{20}Co_{20}Ni_5$ bulk metallic glass. J. Appl. Phys. 115: 223904. doi: 10.1063/1.4882735
19. N. S. Bingham, H. Wang, F. Qin, H. X. Peng, J. F. Sun, V. Franco, H. Srikanth and M. H. Phan (2012) Excellent magnetocaloric properties of melt-extracted Gd-based amorphous microwires. Appl. Phys. Lett. 101:102407. doi: 10.1063/1.4751038
20. L. Xia, Q. Guan, D. Ding, M. B. Tang and Y. D. Dong (2014) Magneto-caloric response of the Gd60Co25Al15 metallic glasses. Appl. Phys. Lett. 105:192402. doi: 10.1063/1.4901263
21. L. Xia, C. Wu, S. H. Chen and K. C. Chan (2015) Magneto-caloric effect of a

$Gd_{50}Co_{50}$ amorphous alloy near the freezing point of water. AIP Adv. 5:097122. doi: 10.1063/1.4930832

22. Z. W. Wang, P. Yu, Y. T. Cui and L. Xia (2016) Near room temperature magneto-caloric effect of a $Gd_{48}Co_{52}$ amorphous alloy. J. Alloy. Compd. 658:598-602. doi: 10.1016/j.jallcom.2015.10.293
23. G. L. Liu, D. Q, Zhao, H. Y. Bai, W. H. Wang and M. X. Pan (2016) Room temperature table-like magnetocaloric effect in amorphous $Gd_{50}Co_{45}Fe_5$ ribbon. J. Phys. D: Appl. Phys. 49:055004. doi: 10.1088/0022-3727/49/5/055004
24. P. Yu, N. Z. Zhang, Y. T. Cui, Z. M. Wu, L. Wen, Z. Y. Zeng and L. Xia (2016) Achieving better magneto-caloric effect near room temperature in amorphous $Gd_{50}Co_{50}$ alloy by minor Zn addition. J. Non-Cryst. Solids. 434:36-40. doi: 10.1016/j.jnoncrysol.2015.12.007
25. S. Chikazumi (1997) Physics of Ferromagnetism, Oxford University Press, New York.
26. J. H. Bloe, J. S. Amaral, A. M. Pereira, V. S. Amaral and J. P. Araujo (2012) On the Curie temperature dependency of the magnetocaloric effect. Appl. Phys. Lett. 100:242407. doi: 10.1063/1.4726110
27. H. Oesterreicher and F. T. Parker (1984) Magnetic cooling near Curie temperatures above 300 K. J. Appl. Phys. 55:4334-4338. doi: 10.1063/1.333046
28. V. Franco, J. M. Borrego, C. F. Conde, A. Conde, M. Stoica, and S. Roth (2006) Refrigerant capacity of FeCrMoCuGaPCB amorphous alloys. J. Appl. Phys. 100:083903. doi: 10.1063/1.2358311